

Article

Exhaustive Photocatalytic Lindane Degradation by Combined Simulated Solar Light-Activated Nanocrystalline TiO₂ and Inorganic Oxidants

Sanullah Khan ^{1,2,3,†}, Changseok Han ^{4,†}, Murtaza Sayed ², Mohammad Sohail ⁵,
Safeer Jan ^{2,6}, Sabiha Sultana ⁷, Hasan M. Khan ² and Dionysios D. Dionysiou ^{3,8,*}

¹ Department of Chemistry, Women University Swabi, Swabi 23430, Pakistan; sukhan3@gmail.com

² Radiation and Environmental Chemistry Laboratory, National Centre of Excellence in Physical Chemistry, University of Peshawar, Peshawar 25120, Pakistan; murtazasayed_407@yahoo.com (M.S.); safeerchemist@yahoo.com (S.J.); hmkhan3@gmail.com (H.M.K.)

³ Environmental Engineering and Science Program, Department of Chemical and Environmental Engineering (ChEE), University of Cincinnati, Cincinnati, OH 45221-0012, USA

⁴ Department of Environmental Engineering, INHA University, Incheon 22212, Korea; hanck@inha.ac.kr

⁵ Institute of Chemical Sciences, University of Swat, Swat 19130, Pakistan; msohail2000@gmail.com

⁶ Hubei Key Laboratory of Electrochemical Power Sources, College of Chemistry and Molecular Sciences, Wuhan University, Wuhan 430072, China

⁷ Department of Chemistry, Islamia College University Peshawar, Peshawar 25120, Pakistan; saba_rehan2006@yahoo.com

⁸ Nireas-International Water Research Centre, University of Cyprus, 1678 Nicosia, Cyprus

* Correspondence: dionysios.d.dionysiou@uc.edu; Tel.: +1-513-556-0724; Fax: +1-513-556-2599

† Contributed equally to this work.

Received: 25 February 2019; Accepted: 8 April 2019; Published: 7 May 2019



Abstract: Organochlorine compounds (OCs) are very toxic, highly persistent, and ubiquitous contaminants in the environment. Degradation of lindane, a selected OC, by simulated solar light-activated TiO₂ (SSLA-TiO₂) photocatalysis was investigated. The film types of the TiO₂ photocatalyst were prepared using a dip-coating method. The physical properties of the films were investigated using X-ray diffraction, transmission electron microscopy, and environmental scanning electron microscopy. The SSLA-TiO₂ photocatalysis led to a lindane removal of 23% in 6 h, with 0.042 h⁻¹ of an observed pseudo first-order rate constant (*k*_{obs}). The SSLA-TiO₂ photocatalysis efficiency was greatly enhanced by adding hydrogen peroxide (H₂O₂), persulfate (S₂O₈²⁻), or both combined, corresponding to a 64%, 89%, and 99% lindane removal in the presence of 200 μM of H₂O₂, S₂O₈²⁻, or equimolar H₂O₂-S₂O₈²⁻, respectively. The hydroxyl and sulfate radicals mainly participated in lindane degradation, proven by the results of a radical scavenger study. The degradation kinetics were hindered in the presence of the water constituents, indicated by a 61%, 35%, 50%, 70%, 88%, and 91% degradation of lindane in 6 h, using a SSLA-TiO₂/S₂O₈²⁻/H₂O₂ photocatalysis system containing 1.0 mg L⁻¹ humic acid (HA), or 1 mM of CO₃²⁻, HCO₃⁻, NO₃⁻, SO₄²⁻, and Cl⁻, respectively. The TiO₂ film demonstrated high reusability during four runs of lindane decomposition experiments. The SSLA-TiO₂/S₂O₈²⁻/H₂O₂ photocatalysis is very effective for the elimination of a persistent OC, lindane, from a water environment.

Keywords: lindane; simulated solar light; TiO₂ photocatalysis; S₂O₈²⁻/H₂O₂; natural water constituents; water treatment

1. Introduction

Many organochlorine compounds (OCs), such as chlorinated alkanes, alkenes, benzenes, phenols, and biphenyls, are often introduced into the environment in the form of solvents, disinfectants, soil fumigants, pesticides, and as dye precursors [1]. A considerable number of OCs also enter the environment as by-products from waste incineration, the chlorination of drinking water and wastewater, and bleaching of pulp with chlorine [2]. OCs are generally considered as very toxic, highly bioaccumulative, and strongly resistant towards biodegradation [2].

Hexachlorocyclohexanes (HCHs) constitute one of the largest classes of chlorinated alkanes that have extensively been used as organochlorine pesticides during the last several decades [3]. The HCHs consist of eight isomers, namely β , γ , δ , θ , ϵ , η , and two α -enantiomers. The insecticidal property of HCHs is solely due to the γ -isomer, commonly known as lindane (i.e., 99% γ -HCH) [4]. The low cost and high efficiency of lindane led to its excessive usage in a wide application range, such as an insecticide and a seed treatment agent in the agricultural and forest industry, a vector control in public health, and as anti-mice and anti-lice agents for livestock and domestic purposes [5,6]. Because of the high chemical stability and mobility of lindane, it ubiquitously disperses in the environment, including biota via the food chain [7]. Owing to the presence of large number of chlorine atoms in the molecule, lindane is a highly toxic compound and is recognized as an endocrine disruptor in the environment [8]. The development of more efficient methods for removing lindane from water is of fundamental importance for environmental cleanup.

Advanced oxidation processes (AOPs) are promising alternatives to the conventional water and wastewater treatment processes, owing to their wide versatility and high efficiency [9]. Among AOPs, TiO_2 photocatalysis is considered as one of the most promising technologies because of the low cost, easy availability, and environmentally benign nature of TiO_2 [10]. The solar light-induced TiO_2 photocatalysis has recently gained much attention in water decontamination and disinfection, owing to the availability and sustainability of sunlight radiation [11,12]. The photocatalytic performance of the catalysts is improved significantly with an increased crystallinity, large surface area, and tailor-designed morphology [13–15]. The efficiency of solar light-activated TiO_2 photocatalytic processes is usually low, because only a small portion of the sunlight (i.e., 5%, namely UV radiation) is involved in the activation of TiO_2 (Reaction (1)) [11].



Hydrogen peroxide (H_2O_2), persulfate ($\text{S}_2\text{O}_8^{2-}$), and, more recently, peroxymonosulfate (HSO_5^-) are emerging inorganic oxidants employed or explored in water and/or wastewater treatment processes, owing to the generation of the strongly reactive oxidants of the hydroxyl radical ($\bullet\text{OH}$) and sulfate radical ($\text{SO}_4^{\bullet-}$) [16–18]. Several inorganic anions (e.g., CO_3^{2-} , HCO_3^- , NO_3^- , SO_4^{2-} , and Cl^-) and organic acids (e.g., humic acid (HA)) are frequently found in water sources, owing to the natural abundances and man-made activities [19]. Depending on the mode of the reaction, these inorganic and organic constituents in water may differently affect the removal efficiency of pollutants using different AOPs [20]. Only limited information is available about the effect of these constituents on the efficiency of combined photocatalytic–photochemical processes, so far.

In this study, the efficiency of a simulated solar light-activated nanocrystalline TiO_2 photocatalyst for decomposing a selected OC, lindane, in an aqueous solution was investigated. The synthesized TiO_2 photocatalyst films were characterized using X-ray diffraction (XRD), environmental scanning electron microscopy (ESEM), and transmission electron microscopy (TEM), for determining its surface morphology and structural properties. The effect of H_2O_2 and $\text{S}_2\text{O}_8^{2-}$ on the activity of the simulated solar light-activated TiO_2 (SSLA- TiO_2) photocatalysis for the removal of lindane was investigated. Radical scavenging experiments were conducted so as to examine the relative importance of the reactive species towards the degradation of lindane. The effect of natural water constituents (i.e., HA and inorganic ions) on the efficiency of the SSLA- $\text{TiO}_2/\text{S}_2\text{O}_8^{2-}/\text{H}_2\text{O}_2$ process was investigated, considering

practical applications. Finally, the performance sustainability of the synthesized TiO₂ photocatalyst was evaluated using four runs of lindane decomposition experiments. The obtained results could provide useful data on the application of SSLA-TiO₂ photocatalysis for removing persistent OCs, such as lindane, from the water environment.

2. Results and Discussion

2.1. Characteristics of Synthesized TiO₂ Films

Figure 1a shows the ESEM image for the film of the TiO₂ photocatalyst. As the film was dried under infrared illumination and then slowly heated up to 350 °C, no cracks in the TiO₂ film were observed at a magnification of 2000×. The peaks of the XRD analysis of the synthesized TiO₂ corresponding to the anatase phase of TiO₂ were observed (Figure 1b). This indicates that the anatase phase of TiO₂ dominated in the films with the synthesis method, based on the observed peaks at 2θ (degree) = 24.8, 37.3, 47.6, 53.5, 55.1, 62.2, 68.8, 70.1, and 74.9, corresponding to the (101), (004), (200), (105), (211), (204), (116), (220), and (215) planes, respectively, of anatase TiO₂ (JCPDS card no. 21-1272). Figure 1c,d shows the HR-TEM images of the sample. The average crystal size of the TiO₂ photocatalyst was 20 ± 5.7 nm. The measured BET surface area was 13.1 ± 0.04 m² g⁻¹ (Figure 1e,f). The spacing between the lattice fringes was calculated as 0.351 nm, similar to the TiO₂ anatase lattice spacing of the (101) plane (i.e., 0.352 nm) [21]. The calculated band-gap energy of the synthesized TiO₂ film by the Kubelka–Munk transformation was 3.1 eV (Figure S1). These results confirmed the formation of the anatase crystalline phase, which has a better photocatalytic activity compared to rutile [22]. The small particle size with the corresponding high surface area, as well as the large number of active sites, could lead to the high photocatalytic activity of the TiO₂ anatase crystalline phase [23]. Lin et al. [24] also reported that the band gap of the TiO₂ nanoparticles is a function of primary particle size, so that when the TiO₂ particle size decreased (i.e., 29 to 17nm), the band gap decreased as well.

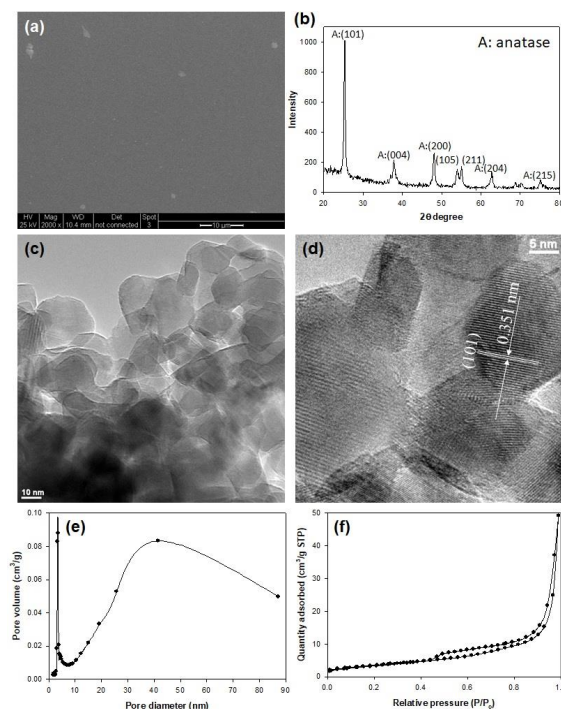


Figure 1. (a) Environmental scanning electron microscopy (ESEM) image of the TiO₂ film, (b) X-ray diffraction (XRD) spectrum of the TiO₂ film, (c,d) high-resolution transmission electron microscopy (HR-TEM) images of the TiO₂ film, (e) pore size distribution, and (f) N₂ adsorption–desorption isotherm of TiO₂ film.

The valence band electrons of the synthesized TiO₂ film are excited to a conduction band when a solar light of sufficient energy illuminates the film. The electrons in the conduction band (e_{CB}^-) interact with oxygen to generate the highly reducing superoxide radical anion ($O_2^{\bullet-}$) (i.e., Reaction (2)), while the valence band holes (h_{VB}^+) react with H₂O or OH⁻ producing the strongly oxidizing \bullet OH, following Reactions (3) and (4), respectively [10].



2.2. SSLA-TiO₂ Photocatalysis of Lindane

Figure 2 shows the degradation of lindane by SSLA-TiO₂ photocatalysis, indicating that 23% lindane was removed in 6 h, corresponding to an observed rate constant (k_{obs}) of 0.042 h⁻¹. Many papers were published on the SSLA-TiO₂ photocatalysis of organic compounds [25–27].

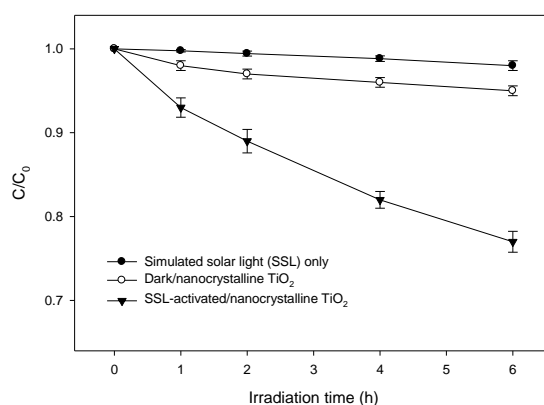


Figure 2. Simulated solar light-activated TiO₂ photocatalysis of lindane. [lindane]₀ = 1.0 μM; mass of TiO₂ film = 9.02 mg; thickness of TiO₂ film = 1.02 μm; area of TiO₂ film = 3750 mm²; pH = 5.8.

The \bullet OH produced in Reactions (3) and (4) was mainly responsible for the decomposition of organic contaminants [28,29]. The $O_2^{\bullet-}$ formed in Reaction (2) might also participate in pollutant degradation, and may likely react with a water molecule to produce additional \bullet OH [30]. Khan et al. [31] previously reported an efficient lindane degradation by \bullet OH, besides a minor lindane removal by $O_2^{\bullet-}$, employing simulated solar light-activated sulfur-doped TiO₂ (S-TiO₂) photocatalysis. In the current case too, it was seen that \bullet OH mainly participated in lindane degradation, although $O_2^{\bullet-}$ also contributed slightly in the degradation process, as will be discussed latter in Section 2.4. Literature studies show that the degradation efficiency of some other organic compounds by solar TiO₂ photocatalysis was rather high [32–34]. The reaction rate constants for the SSLA-TiO₂ photocatalysis of some other pesticides, such as λ-cyhalothrin, chlorpyrifos, and diazinon ($C_0 = 0.1, 0.57, \text{ and } 0.36 \text{ mM}$, respectively) were 0.48, 0.44, and 0.25 h⁻¹, respectively [25]. Adishkumar and Kanmani [26] found that the reaction rate constant for SSLA-TiO₂ photocatalysis of phenol ($C_0 = 1.06 \text{ mM}$) was 1.76 h⁻¹. The apparent discrepancy in the degradation rate constants could be because of the effect of the light intensity [35–37], as well as the molecular structure differences, as previously reported regarding organic pollutants degradation using other AOPs [38]. Parra et al. [36] showed that the degradation efficiency of atrazine using solar simulator/TiO₂ photocatalysis was significantly enhanced by increasing the solar light intensity from 50 to 90 mW/cm². Khataee and Kasiri [39] reported that monoazo dyes have higher photocatalytic degradation rates as compared to the dyes with an anthraquinone structure. The presence of a methyl or chloro group in the dye molecule showed a decreasing effect, while the nitrite group

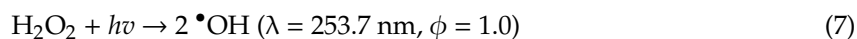
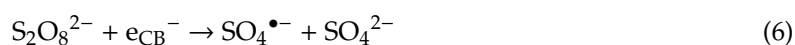
has an increasing effect on the degradation efficiency. The photocatalytic efficiency of dye molecules decreases by a sulfonic substituent, while the hydroxyl group has an opposite effect [39].

Zaleska et al. [40] reported a 77% lindane degradation ($[\text{lindane}]_0 = 0.137 \text{ mM}$; $[\text{TiO}_2]_0 = 0.5 \text{ g/L}$) after 2.5 h irradiation in the anatase TiO_2/UV photocatalytic process. The discrepancy between our results and those reported by Zaleska et al. [40] is in agreement with the findings by Parra et al. [36], showing a higher degradation efficiency of atrazine using UV/TiO_2 than solar simulator/ TiO_2 photocatalysis, obviously due to an efficient activation of TiO_2 for $\bullet\text{OH}$ radical generation by UV than simulated solar light.

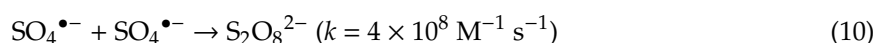
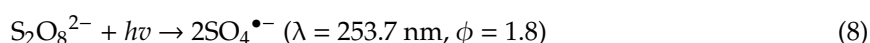
Despite the significant lindane degradation achieved in 6 h, the efficiency of the SSLA- TiO_2 process in the current case may be regarded as low, particularly considering the practical applications. In an attempt to achieve a higher degradation efficiency by SSLA- TiO_2 photocatalysis, inorganic oxidants, such as $\text{S}_2\text{O}_8^{2-}$ and H_2O_2 , were employed as additives in the subsequent experiments, as discussed below.

2.3. Effect of $\text{S}_2\text{O}_8^{2-}$ and H_2O_2 on Lindane Degradation by SSLA- TiO_2 Photocatalysis

Figure 3 shows the effect of $\text{S}_2\text{O}_8^{2-}$ and H_2O_2 on the removal efficiency of lindane using SSLA- TiO_2 photocatalysis. The removal efficiency of lindane was remarkably enhanced by adding 200 μM of $\text{S}_2\text{O}_8^{2-}$ or H_2O_2 , indicated by an 89% and 64% lindane removal in 6 h, corresponding to an observed pseudo first-order rate constant (k_{obs}) of 0.369 and 0.098 h^{-1} , respectively. Both H_2O_2 and $\text{S}_2\text{O}_8^{2-}$ are strong electron acceptors, capable of scavenging the photogenerated e_{CB}^- , according to Reactions (5) and (6), respectively, thus increasing the concentration of $h\nu_{\text{B}}^+$, with a subsequent higher $\bullet\text{OH}$ concentration on the TiO_2 surface [41]. The photolysis of H_2O_2 and $\text{S}_2\text{O}_8^{2-}$ can lead to the generation of additional $\bullet\text{OH}$, as well as $\text{SO}_4^{\bullet-}$, according to Reactions (7) and (8), respectively [42,43]. The above-mentioned phenomena, that is, the promotion of the charge separation followed by an increased production of $\bullet\text{OH}$ and the generation of additional $\bullet\text{OH}$ and $\text{SO}_4^{\bullet-}$, could explain the enhancing effect of H_2O_2 and $\text{S}_2\text{O}_8^{2-}$ [44]. The comparatively higher enhancing effects exerted by the $\text{S}_2\text{O}_8^{2-}$ than H_2O_2 were probably due to an easier activation of $\text{S}_2\text{O}_8^{2-}$ than H_2O_2 by simulated solar radiation containing UV light [45]. The quantum yield results show that the concentration of $\text{SO}_4^{\bullet-}$ generated by the simulated solar radiation (containing UV light) activation of $\text{S}_2\text{O}_8^{2-}$ was high, compared to that of $\bullet\text{OH}$ that resulted from H_2O_2 [46]. Antonopoulou and Konstantinou [47], and Koltzakidou et al. [32] also reported that the addition of $\text{S}_2\text{O}_8^{2-}$ showed a stronger enhancing effect than H_2O_2 on the decomposition of *N,N*-diethyl-*m*-toluamide and cytarabine, respectively, by simulated solar-light assisted TiO_2 photocatalysis.



where " ϕ " is the quantum yield, that is, the number of species formed per photon absorbed.



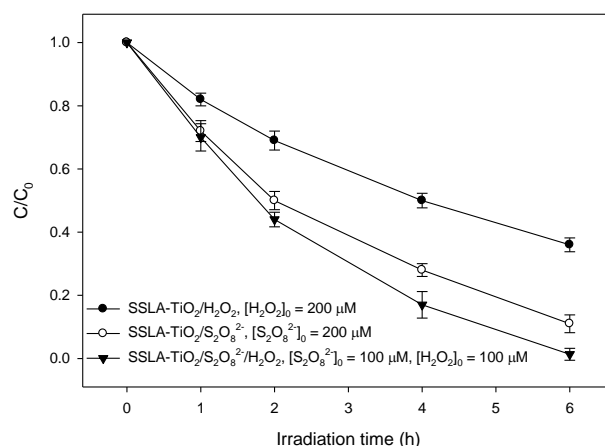


Figure 3. Effect of $S_2O_8^{2-}$ and H_2O_2 additives on the simulated solar light-activated TiO_2 photocatalysis of lindane. $[lindane]_0 = 1.0 \mu M$; $[S_2O_8^{2-}]_0 = [H_2O_2]_0 = 200 \mu M$; mass of TiO_2 film = 9.02 mg; thickness of TiO_2 film = 1.02 μm ; area of TiO_2 film = 3750 mm^2 ; pH = 5.8.

Furthermore, an even stronger enhancing effect on the lindane degradation efficiency (Figure 3) was noticed, indicated by a 99% lindane removal in 6 h, corresponding to a k_{obs} of $0.550 h^{-1}$ when each 100 μM of $S_2O_8^{2-}$ and H_2O_2 was added into the system together. Table 1 shows the kinetics analyses of degradation of various pesticides using TiO_2 photocatalytic processes under different conditions [25,48].

Table 1. Kinetics analyses of degradation of pesticides using different photocatalytic processes.

Pesticides	$k_{obs} (h^{-1})$	Reaction Type	Reference
Vinclozoline	0.408	a	[48]
Quinalphos	0.426	a	[48]
Malathion	4.266	a	[48]
Fenarimol	0.168	a	[48]
Fenitrothion	0.300	a	[48]
Dimethoate	0.666	a	[48]
Lambda-Cyhalothrin	0.504	b	[25]
Chlorpyrifos	0.498	b	[25]
Diazinon	0.270	b	[25]
Lindane	0.550	c	this study

^a Natural sunlight/ $TiO_2/S_2O_8^{2-}$; $[S_2O_8^{2-}]_0 = 250 mg/L$; TiO_2 (P25) = 200 mg/L. ^b Natural sunlight/ TiO_2/H_2O_2 ; $[H_2O_2]_0 = 1000 mg/L$; $TiO_2 = 2.0 g/L$. ^c Simulated solar light/ $TiO_2/S_2O_8^{2-}/H_2O_2$; $[S_2O_8^{2-}]_0 = [H_2O_2]_0 = 100 \mu M$. Mass of TiO_2 film = 9.02 mg; thickness of TiO_2 film = 1.02 μm ; area of TiO_2 film = 3750 mm^2 .

The degradation of organic compounds usually takes place in several steps, involving the generation and destruction of various reaction by-products [49]. The various reaction by-products of lindane identified in the SSLA- $TiO_2/S_2O_8^{2-}/H_2O_2$ process included hexachlorobenzene, tetrachlorocyclohexene, and dichlorophenol, probably resulting via hydrogen abstraction and hydroxylation pathways by using $SO_4^{\bullet-}$ and $\bullet OH$ [20,31]. All of the generated by-products eventually disappeared after 6 h of irradiation. The reactivity of the various by-products generated during the degradation process could be different towards $\bullet OH$ and $SO_4^{\bullet-}$ [50]. For example, chlorobenzene, which is identified in this study as well as frequently reported as a lindane by-product elsewhere using TiO_2 photocatalysis [31,51], typically showed a higher rate constant towards $\bullet OH$ than $SO_4^{\bullet-}$, probably because of the high tendency of the former species for addition reactions due to the multiple bonds [50]. Literature studies show that the efficiency of UV/ $S_2O_8^{2-}$ and UV/ H_2O_2 systems that are capable of generating $SO_4^{\bullet-}$ and $\bullet OH$, respectively, varied when applied to different types of chemical compounds [52,53]. This might explain the larger enhancing effect while using both $S_2O_8^{2-}$ and H_2O_2

combined, because it could provide an opportunity for the different by-products generated to be efficiently degraded under the conditions favorable to it, that is, either $\text{SO}_4^{\bullet-}$ or $\bullet\text{OH}$, or both combined.

Furthermore, the residual oxidant analysis revealed that out of the 100 μM of H_2O_2 and $\text{S}_2\text{O}_8^{2-}$ each employed in the SSLA- $\text{TiO}_2/\text{S}_2\text{O}_8^{2-}/\text{H}_2\text{O}_2$ process, 7 and 23 μM were left as a residue after 6 h of treatment, respectively.

Figure 4 shows the effect of the initial concentration of $\text{S}_2\text{O}_8^{2-}$ and H_2O_2 on the observed pseudo first-order rate constant (k_{obs}) of lindane using the SSLA- TiO_2 photocatalysis. The value of k_{obs} increased at a higher initial $\text{S}_2\text{O}_8^{2-}$ and H_2O_2 concentration, attributable to an increased promotion of the charge separation, as well as the higher concentrations of $\text{SO}_4^{\bullet-}$ and $\bullet\text{OH}$. However, the increase in k_{obs} was less in the case of H_2O_2 than $\text{S}_2\text{O}_8^{2-}$, probably due to the increased recombination rate in the former case, that is, the higher second-order rate constant of Reaction (9) than Reaction (10) [20]. Bekkouche et al. [54] determined an enhancing effect due to an increasing initial concentration of $\text{S}_2\text{O}_8^{2-}$ on the solar-UV/ $\text{TiO}_2/\text{S}_2\text{O}_8^{2-}$ photocatalytic degradation of Safranin O, attributed to an increased generation of reactive radicals. Saïen et al. [45] reported the effects of the initial concentration of $\text{S}_2\text{O}_8^{2-}$ and H_2O_2 using the UV/ TiO_2 photocatalysis of Triton X-100, showing an enhancing effect as a result of increasing the initial concentrations of the oxidants. Koltsakidou et al. [32] reported a decreasing effect as a result of increasing the initial concentrations of H_2O_2 on the SSLA- TiO_2 photocatalytic degradation of cytarabine, attributed to the fast scavenging of $\bullet\text{OH}$ at comparatively higher H_2O_2 concentrations (i.e., 1–4 mM).

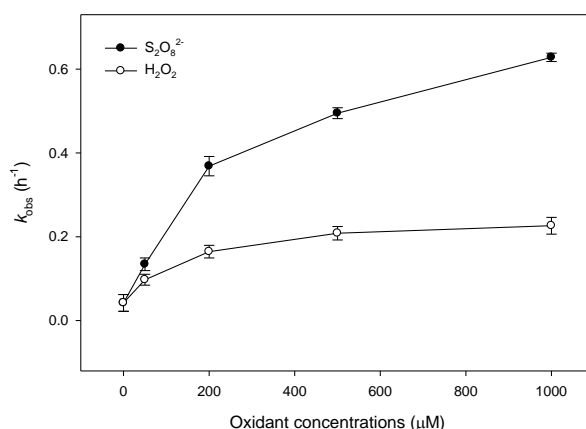


Figure 4. Variation of k_{obs} with increasing initial concentration of $\text{S}_2\text{O}_8^{2-}$ and H_2O_2 on the simulated solar light-activated TiO_2 photocatalysis of lindane. [lindane] $_0 = 1.0 \mu\text{M}$; mass of TiO_2 film = 9.02 mg; thickness of TiO_2 film = 1.02 μm ; area of TiO_2 film = 3750 mm^2 ; pH = 5.8.

2.4. Radical Scavenger Studies and Role of the Reactive Species

The $\bullet\text{OH}$, $\text{SO}_4^{\bullet-}$, and $\text{O}_2^{\bullet-}$ are the main reactive species present in the SSLA- $\text{TiO}_2/\text{S}_2\text{O}_8^{2-}/\text{H}_2\text{O}_2$ system, as discussed above. To identify the role of the individual reactive species in the lindane decomposition, appropriate radical scavenger experiments were performed.

Benzoquinone, tert-butanol, and iso-propanol were employed to scavenge $\text{O}_2^{\bullet-}$, $\bullet\text{OH}$, and both $\bullet\text{OH}$ and $\text{SO}_4^{\bullet-}$, respectively, according to Reactions (11)–(14) [50,55]. In the presence of 50 mM benzoquinone, 89% lindane was decomposed by SSLA- $\text{TiO}_2/\text{S}_2\text{O}_8^{2-}/\text{H}_2\text{O}_2$ in 6 h (Figure 5). In the absence of a radical scavenger, a 99% removal of lindane could be achieved by SSLA- $\text{TiO}_2/\text{S}_2\text{O}_8^{2-}/\text{H}_2\text{O}_2$ in 6 h. The result showed a 10% decrease in the lindane removal efficiency as a result of the addition of benzoquinone, attributable to the reactions of $\text{O}_2^{\bullet-}$. By adding 50 mM tert-butanol, a 58% removal of lindane was achieved in 6 h (Figure 5), indicating a 41% loss in the efficiency of the SSLA- $\text{TiO}_2/\text{S}_2\text{O}_8^{2-}/\text{H}_2\text{O}_2$ system, attributable to the role of $\bullet\text{OH}$. In the presence of 50 mM iso-propanol, only an 11% removal of lindane occurred in 6 h (Figure 5), indicating an 88% decrease in the removal efficiency of lindane by SSLA- $\text{TiO}_2/\text{S}_2\text{O}_8^{2-}/\text{H}_2\text{O}_2$, attributable to the role of the combination of $\bullet\text{OH}$ and $\text{SO}_4^{\bullet-}$. By subtracting, the role of $\bullet\text{OH}$ and $\text{SO}_4^{\bullet-}$ was found to be 41% and 47%, respectively.

The relatively larger contribution of $\text{SO}_4^{\bullet-}$ than $\bullet\text{OH}$ could be due to the high concentration of the former species [45], as well as its high rate constant with lindane [20].

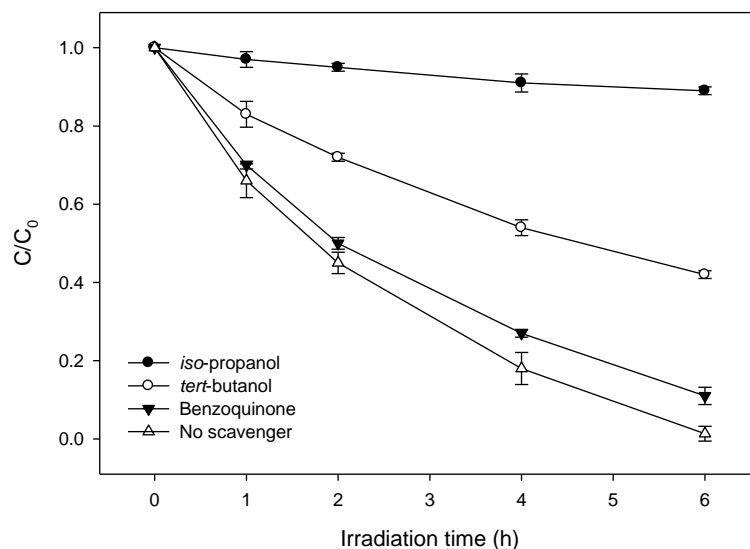
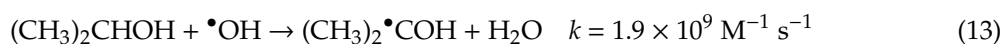
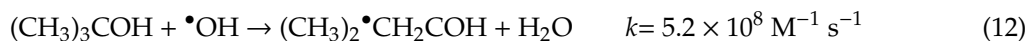
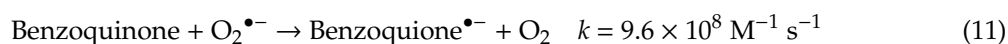


Figure 5. The role of $\bullet\text{OH}$, $\text{SO}_4^{\bullet-}$, and $\text{O}_2^{\bullet-}$ in the simulated solar light-activated $\text{TiO}_2/\text{S}_2\text{O}_8^{2-}/\text{H}_2\text{O}_2$ photocatalysis of lindane. $[\text{lindane}]_0 = 1.0 \mu\text{M}$; $[\text{iso-propanol}]_0 = 50 \text{ mM}$; $[\text{tert-butanol}]_0 = 50 \text{ mM}$; $[\text{benzoquinone}]_0 = 50 \text{ mM}$; mass of TiO_2 film = 9.02 mg; thickness of TiO_2 film = 1.02 μm ; area of TiO_2 film = 3750 mm^2 ; pH = 5.8.

2.5. Influence of Natural Water Constituents

Inorganic ions are one of the most frequently found ingredients in water and wastewater, and are derived from various anthropogenic and non-anthropogenic sources [19]. The presence of inorganic ions can influence the photocatalytic and/or photochemical degradation of organic compounds [56–59]. CO_3^{2-} , HCO_3^- , NO_3^- , SO_4^{2-} , and Cl^- , typical components of natural waters, were selected as inorganic ions in this study. As seen in Figure 6, the efficiency of the SSLA- $\text{TiO}_2/\text{S}_2\text{O}_8^{2-}/\text{H}_2\text{O}_2$ system was reduced by 65%, 50%, 30%, 12%, and 9% in the presence of 1.0 mM of CO_3^{2-} , HCO_3^- , NO_3^- , SO_4^{2-} , and Cl^- , respectively. The inorganic ions could be adsorbed onto the TiO_2 catalyst, thereby decreasing the active site number on its surface [60]. The inhibiting effect may be due to the reduced generation of the reactive radicals owing to the blocking of the TiO_2 active sites [61], as well as the scavenging of the reactive radicals by the ions [59,62]. Liang et al. [58] reported that a degradation rate of the TiO_2 photocatalysis of 2,3-dichlorophenol decreased in the presence of NO_3^- , Cl^- , SO_4^{2-} , and HPO_4^- , attributed to the competitive adsorption on the surface of TiO_2 , besides the scavenging of the $\bullet\text{OH}$ by the ions. Muruganandham and Swaminathan determined that the UV/ TiO_2 photocatalytic oxidation of Reactive Yellow 14 was decreased by adding Cl^- or CO_3^{2-} , attributed to the $\bullet\text{OH}$ scavenging [63]. Our previous study [64] reported a 51%, 34%, 3%, and 1% decrease on the lindane removal efficiency by UV/ HSO_5^- process in the presence of 1.0 mM CO_3^{2-} , HCO_3^- , Cl^- , or SO_4^{2-} , respectively, which was attributed to the scavenging of $\text{SO}_4^{\bullet-}$ and $\bullet\text{OH}$. Contrary to our previous study involving lindane degradation by an UV/ HSO_5^- system [64], the comparatively larger inhibiting effect observed in the current case may indicate an additional TiO_2 deactivation by the ions, besides the scavenging of the

reactive radicals, according to Reactions (15)–(19) [50,65,66]. Despite the high affinity of Cl^- for the scavenging of reactive radicals (Reactions (18) and (19)), a rather small inhibiting effect was observed on the degradation efficiency of lindane. A plausible reason could be the involvement of the reactive Cl^\bullet in the degradation process, as was previously described [20].

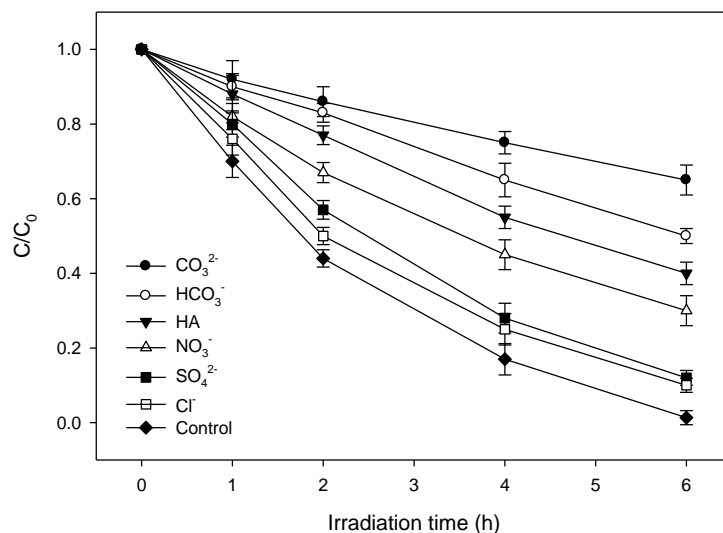
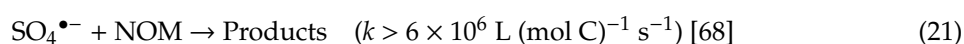
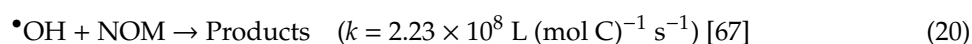
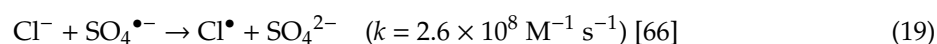
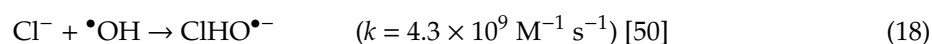
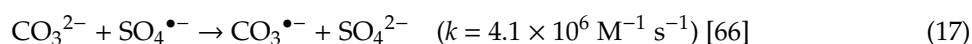
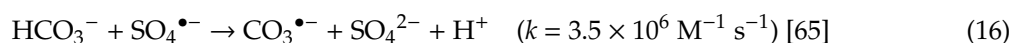
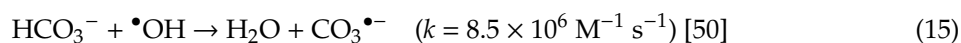


Figure 6. Effect of humic acid and inorganic anions (CO_3^{2-} , HCO_3^- , NO_3^- , SO_4^{2-} , and Cl^-) on the SSLA- $\text{TiO}_2/\text{S}_2\text{O}_8^{2-}/\text{H}_2\text{O}_2$ photocatalysis of lindane. [lindane] $_0 = 1.0 \mu\text{M}$; mass of TiO_2 film = 9.02 mg; thickness of TiO_2 film = 1.02 μm ; area of TiO_2 film = 3750 mm^2 ; [humic acid] $_0 = 1 \text{ mg/L}$; [inorganic ions] $_0 = 1 \text{ mM}$.

The efficiency of lindane degradation by the SSLA- $\text{TiO}_2/\text{S}_2\text{O}_8^{2-}/\text{H}_2\text{O}_2$ process decreased by 39% in the presence of 1.0 mg L^{-1} HA (Figure 6). The result was consistent with the findings of Bekkouche et al. [54], showing that the solar-UV/ $\text{TiO}_2/\text{S}_2\text{O}_8^{2-}$ photocatalytic degradation of Safranin O decreased in the presence of HA. Plausible reasons for the inhibitory effect could be (i) the scavenging of $\bullet\text{OH}$ and $\text{SO}_4^{\bullet-}$ by HA (Reactions (20) and (21)) [67,68], (ii) the blocking of active sites on the TiO_2 surface attributable to HA adsorption [69], and (iii) the absorption of photons by HA [59]. Doorslaer et al. [70] reported that the UV/ TiO_2 photocatalytic degradation rate of moxifloxacin decreased by adding different types of dissolved organic matter (DOM), including HA and fulvic acid, attributed to the scavenging of reactive species (i.e., $\bullet\text{OH}$) as well as the absorption of UV light by DOM. The results might suggest that the natural water constituents studied may adversely affect the efficiency of the $\text{TiO}_2/\text{oxidant}$ -based AOPs applied for the decontamination of field waters, which might need further attention.



2.6. Performance Sustainability of the Synthesized TiO₂ Film

The stability and performance sustainability of the nanocrystalline photocatalyst was tested using the same TiO₂ film for four repeated runs. The percent degradation results achieved by the SSLA-TiO₂/S₂O₈²⁻/H₂O₂ photocatalysis during four successive runs equaled a 99%, 96%, 95%, and 93% lindane removal in 6 h (Figure 7). The obtained results might indicate a high performance sustainability for the synthesized TiO₂ film under the experimental condition in this study. Han et al. [56] and Pelaez et al. [71] reported a similar performance sustainability using nanocrystalline S-TiO₂, and nitrogen and fluorine doped TiO₂ (NF-TiO₂) photocatalysts, respectively, synthesized via a similar method. Hung et al. [72] recently reported that the sol-gel synthesized doped-TiO₂ exhibited a higher reusability than the film synthesized by a hydrothermal method, attributable to the high calcinations temperature in the former case. The high activity and reusability may recommend the synthesized TiO₂ photocatalyst as a promising choice for application purposes.

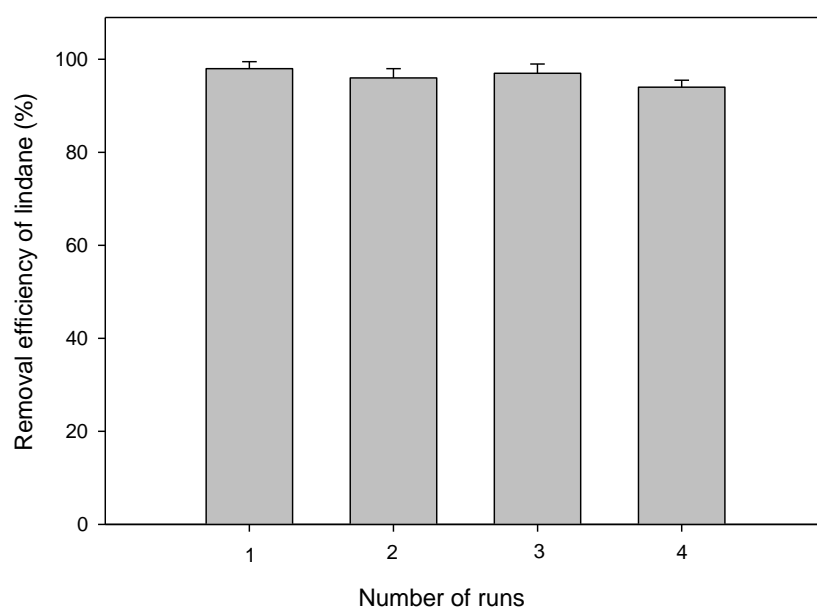


Figure 7. Test of reusability for the simulated solar light-activated TiO₂/S₂O₈²⁻/H₂O₂ photocatalyst of lindane. [lindane]₀ = 1.0 μM; mass of TiO₂ film = 9.02 mg; thickness of TiO₂ film = 1.02 μm; area of TiO₂ film = 3750 mm²; pH = 5.8.

3. Materials and Methods

3.1. Materials

Titanium (IV) isopropoxide (TTIP; 97%), lindane (C₆H₆Cl₆; 97%), and persulfate (S₂O₈²⁻) were obtained from Sigma-Aldrich (St. Louis, MO, USA). Acetic acid (CH₃COOH, HAc), hydrogen peroxide (H₂O₂, 50%, v/v), sodium carbonate (Na₂CO₃), sodium chloride (NaCl), sodium nitrate (NaNO₃), sodium bicarbonate (NaHCO₃), isopropyl alcohol (i-PrOH; Certified ACS), and sodium sulfate (Na₂SO₄) were purchased from Fisher Scientific (Hampton, NH, United States). For a reference natural organic matter (NOM) in this study, standard Suwannee River humic acid (SRHA) was obtained from the International Humic Substances Society (IHSS, University of Minnesota, St. Paul, MN, USA). Benzoquinone (C₆H₄O₂, BQ), iso-propanol ((CH₃)₂CHOH), and tert-butanol (CH₃)₃COH) were used as radical scavengers and were obtained from ACROS Organics (Morris, NJ, USA). Milli-Q grade water (resistivity: 18.2 MΩ cm) was used to prepare the aqueous solutions during the experiments. All of the chemicals were used without further treatment.

3.2. TiO₂ Film Preparation

The preparation of film types of TiO₂ photocatalyst was performed with a dip-coating technique using a TiO₂ solution, and according to the procedure described in our previous paper [56]. In short, the TTIP was dissolved in *i*-PrOH, and then acetic acid was added in the solution. The solution was kept under vigorous stirring for 24 h at room temperature. As a result, a stable solution was obtained with a white color. The molar ratio of *i*-PrOH:TTIP:HAc was 45:1:1. The synthesized TiO₂ material was immobilized on a glass substrate (Gold Seal[®] Micro Slides (75 × 25mm; 1mm thick), Portsmouth, NH, USA) in a five-layered nanocrystalline thin film employing a dip-coating method. After the coating process, the film was dried under infrared illumination for 20 min, and then calcined at 350 °C for 2 h in a Paragon HT-22-D furnace (Thermcraft Inc., Winston-Salem, NC, USA). The temperature of 350 °C was chosen so as to avoid the formation of cracks as a result of the high stress towards the coating during the calcination process. Also, at the relatively low calcination temperature, the phase transformation from anatase to rutile, as well as the collapse of porous structure of the film were inhibited during the film preparation. The thickness of the prepared film was $1.02 \pm 0.02 \mu\text{m}$ and the total mass of the immobilized TiO₂ was $4.51 \pm 0.18 \text{ mg}$.

3.3. Characterization of Synthesized TiO₂ Films

The characterization techniques used in this study were similar to those in our previously published paper [56]. Briefly, the surface morphology of the synthesized TiO₂ photocatalyst film was characterized using an ESEM (Philips XL 30ESEM-FEG, Eindhoven, The Netherlands). The crystal size and crystal structure of the TiO₂ photocatalyst were characterized using a JEM-2010F high resolution-TEM (HR-TEM, JEOL, Tokyo, Japan) with a field emission gun at 200 kV. An X-ray diffraction (XRD) analysis was performed using a X'Pert PRO XRD diffractometer (Philips, Almelo, The Netherlands) with Cu K α radiation ($\lambda = 1.5406 \text{ \AA}$) so as to examine the crystal structures of TiO₂ photocatalyst. The light absorption property of synthesized TiO₂ film was investigated using a Shimadzu 2501 PC UV-visible spectrophotometer equipped with an ISR 1200 integrated sphere attachment. The reference material for the analysis was BaSO₄. The Brunauer, Emmett, and Teller (BET) surface area of the sample was measured with a Micromeritics Tristar 3000 (Norcross, GA, USA). For the XRD, BET, UV-visible light absorption, and HR-TEM analyses, powders from the TiO₂ coatings were collected using a blade, which were then used for analysis.

3.4. Photocatalytic Experiments

The photocatalytic experiments were performed in a batch mode photoreactor of a borosilicate glass Petri dish with a diameter of 10 cm. For the UV transmission, a quartz cover was used. A 20 mL aqueous solution of lindane (1 μM) at pH 5.8 and containing two thin film-coated TiO₂ slides was irradiated with simulated solar light in the photoreactor. In the experiments concerning the effects of oxidants or natural water constituents on lindane degradation, desired amounts of the chemicals (i.e., 100 μM S₂O₈²⁻ or H₂O₂, 1 mM inorganic ions, and 1 mg/L HA) were added to the lindane solution at the start of the experiment. A 300 W Xenon lamp (Newport, Oriel Instrument, Irvine, CA, USA) emitted simulated solar light radiation. The wavelength of the solar light was mainly from 330 to 760 nm. A schematic diagram of the photocatalytic experimentation is shown in Figure 8. The measured light irradiance (E_e) using a Newport broadband radiant power meter was $4.71 \times 10^{-2} \text{ W cm}^{-2}$. The experiments were repeated at least three times.

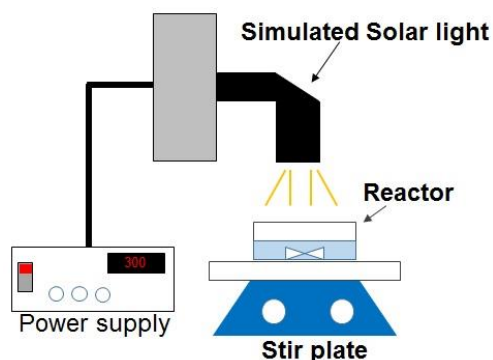


Figure 8. A schematic diagram of the photocatalytic experimental procedure.

3.5. Analytical Methods

The lindane concentration was monitored using an Agilent 6890 gas chromatograph (GC; Wilmington, DE, USA) with an Agilent 5975 mass spectrometer (MS; Wilmington, DE, USA), using the method previously reported in our study [64]. Briefly, a solid phase micro extraction (SPME) technique was used for the sample extraction. An HP-5MS (5% phenyl methylsiloxane) capillary column (length: 30 m and i.d.: 0.25 μm) was employed for the separation of the analyte. The mass spectra of the compounds in the samples were obtained in an electron impact ionization mode (EI^+) at 70 eV, with an m/z ranging from 50 to 550. An online mass spectral search program (National Institute of Standards and Technology (NIST), Gaithersburg, MD, USA, <https://www.nist.gov/>) was used to interpret the obtained mass spectra using the GC-MS. For the residual analysis of H_2O_2 and $\text{S}_2\text{O}_8^{2-}$, two colorimetric methods, described by Liang et al. [73] and Allen et al. [74], were used.

4. Conclusions

The efficiency of a sustainable technology employing solar photocatalysis for the elimination of lindane, a persistent organochlorine compound, from an aqueous solution was evaluated using a sol-gel synthesized nanocrystalline TiO_2 photocatalyst film. The results of the ESEM and TEM analyses showed a highly uniform and smooth surface morphology comprising anatase as the dominant crystalline phase in the TiO_2 film. The synthesized TiO_2 photocatalyst decomposed 23% lindane in 6 h, reflecting a limited lower removal efficiency in a practical application. Meanwhile, the efficiency of the SSLA- TiO_2 photocatalysis was remarkably improved by the addition of environmentally friendly and economically attractive oxidants (i.e., $\text{S}_2\text{O}_8^{2-}$ or H_2O_2), achieving an 89% and 64% removal of lindane, respectively, in 6 h. The removal efficiency of lindane further increased by 10% when using an equimolar mixture of both of the oxidants simultaneously (i.e., $\text{S}_2\text{O}_8^{2-}$ and H_2O_2), which corresponds to a 99% removal within 6 h. The $\text{SO}_4^{\bullet-}$ and $\bullet\text{OH}$ were mostly involved in lindane degradation using an SSLA- $\text{TiO}_2/\text{S}_2\text{O}_8^{2-}/\text{H}_2\text{O}_2$ system. The lindane removal efficiency for the SSLA- $\text{TiO}_2/\text{S}_2\text{O}_8^{2-}/\text{H}_2\text{O}_2$ process decreased significantly in the presence of natural water constituents (i.e., HA, CO_3^{2-} , HCO_3^- , NO_3^- , SO_4^{2-} , and Cl^-), requiring a high energy input in the contaminated field water treatment processes. The sustained catalytic activity of the TiO_2 film during four runs manifested a high stability and reusability of the synthesized photocatalyst. The SSLA- $\text{TiO}_2/\text{S}_2\text{O}_8^{2-}/\text{H}_2\text{O}_2$ is very effective for the elimination of lindane, and potentially other OCs, from a water environment. Importantly, as the remaining $\text{S}_2\text{O}_8^{2-}$ in the process after the complete removal of OCs may result in secondary contamination [75,76], the $\text{S}_2\text{O}_8^{2-}$ concentration must be kept as low as possible in order to treat the OCs in the process. It may be the limitations of the SSLA- $\text{TiO}_2/\text{S}_2\text{O}_8^{2-}/\text{H}_2\text{O}_2$ system for practical applications.

Supplementary Materials: The following are available online at <http://www.mdpi.com/2073-4344/9/5/425/s1>. Figure S1: Tauc plot of Kubelka–Munk transformation of synthesized TiO_2 films. Inserts shows the UV-visible absorption spectrum of the TiO_2 film.

Author Contributions: Planning and designing of the research was made by S.K. and C.H. The experiments were performed by S.K. Materials were synthesized and characterized by S.K. and C.H. Drafting of manuscript

was done by S.K., C.H., M.S., S.J. and S.S. Critical revision was performed by D.D.D. and H.M.K. Planning and supervision of the research was made by Dionysiou D.D.D.

Funding: This research was funded by Women University, Swabi, Pakistan. The APC was funded by the Cyprus Research Promotion Foundation through Desmi 2009–2010, which is co-funded by the Republic of Cyprus and ERDF under contract number NEA IPODOMI/STRATH/0308/09.

Acknowledgments: The authors are thankful to Dominic L. Boccelli of the University of Cincinnati (UC) for allowing us to use the GC-MS. We acknowledge the financial assistance from the Women University, Swabi, Pakistan. We also acknowledge the financial support from the Cyprus Research Promotion Foundation through Desmi 2009–2010, which is co-funded by the Republic of Cyprus and ERDF under contract number NEA IPODOMI/STRATH/0308/09. Also, D.D. Dionysiou acknowledges support from the UC through a UNESCO co-Chair Professor position on “Water Access and Sustainability”, and the Herman Schneider Professorship in the College of Engineering and Applied Sciences.

Conflicts of Interest: The authors declare no conflict of interest.

References

1. Lin, S.; Su, G.; Zheng, M.; Jia, M.; Qi, C.; Li, W. The degradation of 1,2,4-trichlorobenzene using synthesized Co_3O_4 and the hypothesized mechanism. *J. Hazard. Mater.* **2011**, *192*, 1697–1704. [[CrossRef](#)]
2. Movahedyan, H.; Mohammadi, A.S.; Assadi, A. Comparison of different advanced oxidation processes degrading p-chlorophenol in aqueous solution. *J. Environ. Health Sci. Eng.* **2009**, *6*, 153–160.
3. Li, S.; Elliott, D.W.; Spear, S.T.; Ma, L.; Zhang, W.-X. Hexachlorocyclohexanes in the Environment: Mechanisms of Dechlorination. *Crit. Rev. Environ. Sci. Technol.* **2011**, *41*, 1747–1792. [[CrossRef](#)]
4. Okeke, B.C.; Siddique, T.; Arbestain, M.C.; Frankenberger, W.T. Biodegradation of gamma-hexachlorocyclohexane (lindane) and alpha-hexachlorocyclohexane in water and a soil slurry by a *Pandoraea* species. *J. Agric. Food Chem.* **2002**, *50*, 2548–2555. [[CrossRef](#)] [[PubMed](#)]
5. Bhatt, P.; Kumar, M.S.; Chakrabarti, T. Assessment of bioremediation possibilities of technical grade hexachlorocyclohexane (tech-HCH) contaminated soils. *J. Hazard. Mater.* **2007**, *143*, 349–353. [[CrossRef](#)] [[PubMed](#)]
6. Hardie, D.W.F. Benzene hexachloride. In *Encyclopedia of Chemical Technology*, 2nd ed.; Kirk, R.E., Othmer, D.F., Eds.; John Wiley & Sons: New York, NY, USA, 1964; Volume 5, pp. 267–281.
7. Begum, A.; Gautam, S.K. Dechlorination of endocrine disrupting chemicals using $\text{Mg}_0/\text{ZnCl}_2$ bimetallic system. *Water Res.* **2011**, *45*, 2383–2391. [[CrossRef](#)]
8. Pant, N.; Shukla, M.; Upadhyay, A.; Chaturvedi, P.; Saxena, D.; Gupta, Y. Association between environmental exposure to p, p'-DDE and lindane and semen quality. *Environ. Sci. Pollut. Res.* **2014**, *21*, 11009–11016. [[CrossRef](#)] [[PubMed](#)]
9. Evgenidou, E.; Konstantinou, I.; Fytianos, K.; Poullos, I. Oxidation of two organophosphorous insecticides by the photo-assisted Fenton reaction. *Water Res.* **2007**, *41*, 2015–2027. [[CrossRef](#)] [[PubMed](#)]
10. Hoffmann, M.R.; Martin, S.T.; Choi, W.; Bahnemann, D.W. Environmental Applications of Semiconductor Photocatalysis. *Chem. Rev.* **1995**, *95*, 69–96. [[CrossRef](#)]
11. Malato, S.; Fernández-Ibáñez, P.; Maldonado, M.I.; Blanco, J.; Gernjak, W. Decontamination and disinfection of water by solar photocatalysis: Recent overview and trends. *Catal. Today* **2009**, *147*, 1–59. [[CrossRef](#)]
12. Byrne, J.A.; Fernandez-Ibanez, P.A.; Dunlop, P.S.; Alrousan, D.; Hamilton, J.W. Photocatalytic Enhancement for Solar Disinfection of Water: A Review. *Int. J. Photoenergy* **2011**, *2011*, 798051. [[CrossRef](#)]
13. Park, C.H.; Lee, C.M.; Choi, J.W.; Park, G.C.; Joo, J. Enhanced photocatalytic activity of porous single crystal TiO_2/CNT composites by annealing process. *Ceram. Int.* **2018**, *44*, 1641–1645. [[CrossRef](#)]
14. Chandran, K.; Kait, C.F.; Zaid, H.F.M. Morphology of titanium dioxide synthesized via precipitation technique: Effect of calcination and reflux on the surface morphology. *J. Phys. Conf. Ser.* **2018**, *1123*, 012059. [[CrossRef](#)]
15. Ghosh, M.; Liu, J.; Chuang, S.S.; Jana, S.C. Fabrication of hierarchical V_2O_5 nanorods on TiO_2 nanofibers and their enhanced photocatalytic activity under visible light. *ChemCatChem* **2018**, *10*, 3305–3318. [[CrossRef](#)]
16. Shah, N.S.; He, X.; Khan, H.M.; Khan, J.A.; O'Shea, K.E.; Boccelli, D.L.; Dionysiou, D.D. Efficient removal of endosulfan from aqueous solution by UV-C/peroxides: A comparative study. *J. Hazard. Mater.* **2013**, *263 Pt 2*, 584–592. [[CrossRef](#)]

17. Khan, J.A.; He, X.; Khan, H.M.; Shah, N.S.; Dionysiou, D.D. Dionysiou, Oxidative degradation of atrazine in aqueous solution by UV/H₂O₂/Fe²⁺, UV/S₂O₈²⁻/Fe²⁺ and UV/HSO₅⁻/Fe²⁺ processes: A comparative study. *Chem. Eng. J.* **2013**, *218*, 376–383. [[CrossRef](#)]
18. Boczkaj, G.; Fernandes, A. Wastewater treatment by means of Advanced Oxidation Processes at basic pH conditions: A review. *Chem. Eng. J.* **2017**, *320*, 608–633. [[CrossRef](#)]
19. Sayed, M.; Ismail, M.; Khan, S.; Tabassum, S.; Khan, H.M. Degradation of ciprofloxacin in water by advanced oxidation process: Kinetics study, influencing parameters and degradation pathways. *Environ. Technol.* **2016**, *37*, 590–602. [[CrossRef](#)]
20. Khan, S.; He, X.; Khan, J.A.; Khan, H.M.; Boccelli, D.L.; Dionysiou, D.D. Kinetics and mechanism of sulfate radical- and hydroxyl radical-induced degradation of highly chlorinated pesticide lindane in UV/peroxymonosulfate system. *Chem. Eng. J.* **2017**, *318*, 135–142. [[CrossRef](#)]
21. Dai, S.; Wu, Y.; Sakai, T.; Du, Z.; Sakai, H.; Abe, M. Preparation of Highly Crystalline TiO₂ Nanostructures by Acid-assisted Hydrothermal Treatment of Hexagonal-structured Nanocrystalline Titania/Cetyltrimethylammonium Bromide Nanoskeleton. *Nanoscale Res. Lett.* **2010**, *5*, 1829–1835. [[CrossRef](#)]
22. Helali, S.; Polo-López, M.I.; Fernández-Ibáñez, P.; Ohtani, B.; Amano, F.; Malato, S.; Guillard, C. Solar photocatalysis: A green technology for E. coli contaminated water disinfection. Effect of concentration and different types of suspended catalyst. *J. Photochem. Photobiol. A Chem.* **2014**, *276*, 31–40. [[CrossRef](#)]
23. Herrmann, J.-M. Heterogeneous photocatalysis: Fundamentals and applications to the removal of various types of aqueous pollutants. *Catal. Today* **1999**, *53*, 115–129. [[CrossRef](#)]
24. Lin, H.; Huang, C.P.; Li, W.; Ni, C.; Shah, S.I.; Tseng, Y.H. Size dependency of nanocrystalline TiO₂ on its optical property and photocatalytic reactivity exemplified by 2-chlorophenol. *Appl. Catal. B Environ.* **2006**, *68*. [[CrossRef](#)]
25. Alalm, M.G.; Tawfik, A.; Ookawara, S. Comparison of solar TiO₂ photocatalysis and solar photo-Fenton for treatment of pesticides industry wastewater: Operational conditions, kinetics, and costs. *J. Water Process Eng.* **2015**, *8*, 55–63. [[CrossRef](#)]
26. Adishkumar, S.; Kanmani, S. Treatment of phenolic wastewaters in single baffle reactor by Solar/TiO₂/H₂O₂ process. *Desalin. Water Treat.* **2010**, *24*, 67–73. [[CrossRef](#)]
27. Pelizzetti, E.; Borgarello, M.; Minero, C.; Pramauro, E.; Borgarello, E.; Serpone, N. Photocatalytic degradation of polychlorinated dioxins and polychlorinated biphenyls in aqueous suspensions of semiconductors irradiated with simulated solar light. *Chemosphere* **1988**, *17*, 499–510. [[CrossRef](#)]
28. Robert, D.; Malato, S. Solar photocatalysis: A clean process for water detoxification. *Sci. Total Environ.* **2002**, *291*, 85–97. [[CrossRef](#)]
29. Oller, I.; Gernjak, W.; Maldonado, M.; Pérez-Estrada, L.; Sánchez-Pérez, J.; Malato, S. Solar photocatalytic degradation of some hazardous water-soluble pesticides at pilot-plant scale. *J. Hazard. Mater.* **2006**, *138*, 507–517. [[CrossRef](#)] [[PubMed](#)]
30. Pelaez, M.; Nolan, N.T.; Pillai, S.C.; Seery, M.K.; Falaras, P.; Kontos, A.G.; Dunlop, P.S.M.; Hamilton, J.W.J.; Byrne, J.A.; O'Shea, K.; et al. A review on the visible light active titanium dioxide photocatalysts for environmental applications. *Appl. Catal. B Environ.* **2012**, *125*, 331–349. [[CrossRef](#)]
31. Khan, S.; Han, C.; Khan, H.M.; Boccelli, D.L.; Nadagouda, M.N.; Dionysiou, D.D. Efficient degradation of lindane by visible and simulated solar light-assisted S-TiO₂/peroxymonosulfate process: Kinetics and mechanistic investigations. *J. Mol. Catal. A Chem.* **2017**, *428*, 9–16. [[CrossRef](#)]
32. Koltsakidou, A.; Antonopoulou, M.; Evgenidou, E.; Konstantinou, I.; Lambropoulou, D. Cytarabine degradation by simulated solar assisted photocatalysis using TiO₂. *Chem. Eng. J.* **2017**, *316*, 823–831. [[CrossRef](#)]
33. Borges, M.; Sierra, M.; Méndez-Ramos, J.; Acosta-Mora, P.; Ruiz-Morales, J.; Esparza, P. Solar degradation of contaminants in water: TiO₂ solar photocatalysis assisted by up-conversion luminescent materials. *Sol. Energy Mater. Sol. Cells* **2016**, *155*, 194–201. [[CrossRef](#)]
34. De la Cruz, N.; Dantas, R.; Giménez, J.; Esplugas, S. Photolysis and TiO₂ photocatalysis of the pharmaceutical propranolol: Solar and artificial light. *Appl. Catal. B Environ.* **2013**, *130*, 249–256. [[CrossRef](#)]
35. Bhatkhande, D.S.; Pangarkar, V.G.; Beenackers, A.A.C.M. Photocatalytic degradation for environmental applications—A review. *J. Chem. Technol. Biotechnol.* **2002**, *77*, 102–116. [[CrossRef](#)]
36. Parra, S.; Stanca, S.E.; Guasaquillo, I.; Thampi, K.R. Photocatalytic degradation of atrazine using suspended and supported TiO₂. *Appl. Catal. B Environ.* **2004**, *51*, 107–116. [[CrossRef](#)]

37. Khan, S.; Sayed, M.; Sohail, M.; Shah, L.A.; Raja, M.A. Advanced Oxidation and Reduction Processes. In *Advances in Water Purification Techniques*; Elsevier: Amsterdam, The Netherlands, 2019; pp. 135–164. [[CrossRef](#)]
38. Getoff, N. Factors influencing the efficiency of radiation-induced degradation of water pollutants. *Radiat. Phys. Chem.* **2002**, *65*, 437–446. [[CrossRef](#)]
39. Khataee, A.; Kasiri, M.B. Photocatalytic degradation of organic dyes in the presence of nanostructured titanium dioxide: Influence of the chemical structure of dyes. *J. Mol. Catal. A Chem.* **2010**, *328*, 8–26. [[CrossRef](#)]
40. Zaleska, A.; Hupka, J.; Wiergowski, M.; Biziuk, M. Photocatalytic degradation of lindane, p,p'-DDT and methoxychlor in an aqueous environment. *J. Photochem. Photobiol. A Chem.* **2000**, *135*, 213–220. [[CrossRef](#)]
41. Koltsakidou, A.; Antonopoulou, M.; Evgenidou, E.; Konstantinou, I.; Giannakas, A.; Papadaki, M.; Bikiaris, D.; Lambropoulou, D.A. Photocatalytic removal of fluorouracil using TiO₂-P25 and N/S doped TiO₂ catalysts: A kinetic and mechanistic study. *Sci. Total Environ.* **2017**, *578*, 257–267. [[CrossRef](#)] [[PubMed](#)]
42. Khandarkhaeva, M.; Batoeva, A.; Aseev, D.; Sizykh, M.; Tsydenova, O. Oxidation of atrazine in aqueous media by solar-enhanced Fenton-like process involving persulfate and ferrous ion. *Ecotoxicol. Environ. Saf.* **2017**, *137*, 35–41. [[CrossRef](#)] [[PubMed](#)]
43. Anipsitakis, G.P.; Dionysiou, D.D. Transition metal/UV-based advanced oxidation technologies for water decontamination. *Appl. Catal. B Environ.* **2004**, *54*, 155–163. [[CrossRef](#)]
44. Kositzi, M.; Poulis, I.; Malato, S.; Caceres, J.; Campos, A. Campos, Solar photocatalytic treatment of synthetic municipal wastewater. *Water Res.* **2004**, *38*, 1147–1154. [[CrossRef](#)] [[PubMed](#)]
45. Saien, J.; Ojaghloo, Z.; Soleymani, A.; Rasoulifard, M. Homogeneous and heterogeneous AOPs for rapid degradation of Triton X-100 in aqueous media via UV light, nanotitania hydrogen peroxide and potassium persulfate. *Chem. Eng. J.* **2011**, *167*, 172–182. [[CrossRef](#)]
46. Olmez-Hanci, T.; Dursun, D.; Aydin, E.; Arslan-Alaton, I.; Girit, B.; Mita, L.; Diano, N.; Mita, D.G.; Guida, M. S₂O₈²⁻/UV-C and H₂O₂/UV-C treatment of Bisphenol A: Assessment of toxicity, estrogenic activity, degradation products and results in real water. *Chemosphere* **2015**, *119*, S115–S123. [[CrossRef](#)] [[PubMed](#)]
47. Antonopoulou, M.; Konstantinou, I. Effect of oxidants in the photocatalytic degradation of DEET under simulated solar irradiation in aqueous TiO₂ suspensions. *Glob. NEST J.* **2014**, *16*, 507–515. [[CrossRef](#)]
48. Vela, N.; Calín, M.; Yáñez-Gascón, M.J.; Garrido, I.; Pérez-Lucas, G.; Fenoll, J.; Navarro, S. Photocatalytic oxidation of six pesticides listed as endocrine disruptor chemicals from wastewater using two different TiO₂ samples at pilot plant scale under sunlight irradiation. *J. Photochem. Photobiol. A Chem.* **2018**, *353*, 271–278. [[CrossRef](#)]
49. Burrows, H.D.; Santaballa, J.; Steenken, S. Reaction pathways and mechanisms of photodegradation of pesticides. *J. Photochem. Photobiol. B Biol.* **2002**, *67*, 71–108. [[CrossRef](#)]
50. Buxton, G.V.; Greenstock, C.L.; Helman, W.P.; Ross, A.B. Critical Review of rate constants for reactions of hydrated electrons, hydrogen atoms and hydroxyl radicals ($\bullet\text{OH}/\bullet\text{O}^-$ in Aqueous Solution. *J. Phys. Chem. Ref. Data* **1988**, *17*, 513–886. [[CrossRef](#)]
51. Antonaraki, S.; Triantis, T.; Papaconstantinou, E.; Hiskia, A. Photocatalytic degradation of lindane by polyoxometalates: Intermediates and mechanistic aspects. *Catal. Today* **2010**, *151*, 119–124. [[CrossRef](#)]
52. Tan, C.; Gao, N.; Deng, Y.; Zhang, Y.; Sui, M.; Deng, J.; Zhou, S. Degradation of antipyrine by UV, UV/H₂O₂ and UV/PS. *J. Hazard. Mater.* **2013**, *260*, 1008–1016. [[CrossRef](#)]
53. Kwon, M.; Kim, S.; Yoon, Y.; Jung, Y.; Hwang, T.-M.; Lee, J.; Kang, J.-W. Comparative evaluation of ibuprofen removal by UV/H₂O₂ and UV/S₂O₈²⁻ processes for wastewater treatment. *Chem. Eng. J.* **2015**, *269*, 379–390. [[CrossRef](#)]
54. Bekkouche, S.; Merouani, S.; Hamdaoui, O.; Bouhelassa, M. Efficient photocatalytic degradation of Safranin O by integrating solar-UV/TiO₂/persulfate treatment: Implication of sulfate radical in the oxidation process and effect of various water matrix components. *J. Photochem. Photobiol. A Chem.* **2017**, *345*, 80–91. [[CrossRef](#)]
55. Wu, X.; Gu, X.; Lu, S.; Xu, M.; Zang, X.; Miao, Z.; Qiu, Z.; Sui, Q. Degradation of trichloroethylene in aqueous solution by persulfate activated with citric acid chelated ferrous ion. *Chem. Eng. J.* **2014**, *255*, 585–592. [[CrossRef](#)]
56. Han, C.; Pelaez, M.; Likodimos, V.; Kontos, A.G.; Falaras, P.; O'Shea, K.; Dionysiou, D.D. Innovative visible light-activated sulfur doped TiO₂ films for water treatment. *Appl. Catal. B Environ.* **2011**, *107*, 77–87. [[CrossRef](#)]

57. Kanakaraju, D.; Motti, C.A.; Glass, B.D.; Oelgemöller, M. TiO₂ photocatalysis of naproxen: Effect of the water matrix, anions and diclofenac on degradation rates. *Chemosphere* **2015**, *139*, 579–588. [[CrossRef](#)]
58. Liang, H.-C.; Li, X.-Z.; Yang, Y.-H.; Sze, K.-H. Effects of dissolved oxygen, pH, and anions on the 2, 3-dichlorophenol degradation by photocatalytic reaction with anodic TiO₂ nanotube films. *Chemosphere* **2008**, *73*, 805–812. [[CrossRef](#)] [[PubMed](#)]
59. Simmons, M.S.; Zepp, R.G. Influence of humic substances on photolysis of nitroaromatic compounds in aqueous systems. *Water Res.* **1986**, *20*, 899–904. [[CrossRef](#)]
60. Zhu, X.; Nanny, M.A.; Butler, E.C. Effect of inorganic anions on the titanium dioxide-based photocatalytic oxidation of aqueous ammonia and nitrite. *J. Photochem. Photobiol. A Chem.* **2007**, *185*, 289–294. [[CrossRef](#)]
61. Niessner, R. Photocatalytic Atrazine Degradation by Synthetic Minerals, Atmospheric Aerosols, and Soil Particles. *Environ. Sci. Technol.* **2002**, *36*, 5342–5347. [[CrossRef](#)]
62. Xia, X.-H.; Xu, J.-L.; Yun, Y. Effects of common inorganic anions on the rates of photocatalytic degradation of sodium dodecylbenzenesulfonate over illuminated titanium dioxide. *J. Environ. Sci.* **2002**, *14*, 188–194.
63. Muruganandham, M.; Swaminathan, M. TiO₂–UV photocatalytic oxidation of Reactive Yellow 14: Effect of operational parameters. *J. Hazard. Mater.* **2006**, *135*, 78–86. [[CrossRef](#)]
64. Khan, S.; He, X.; Khan, H.M.; Boccelli, D.; Dionysiou, D.D. Efficient degradation of lindane in aqueous solution by iron (II) and/or UV activated peroxy monosulfate. *J. Photochem. Photobiol. A Chem.* **2016**, *316*, 37–43. [[CrossRef](#)]
65. Huie, R.E.; Clifton, C.L. Temperature dependence of the rate constants for reactions of the sulfate radical, SO₄^{•−}, with anions. *J. Phys. Chem.* **1990**, *94*, 8561–8567. [[CrossRef](#)]
66. Padmaja, S.; Neta, P.; Huie, R. Rate constants for some reactions of inorganic radicals with inorganic ions. Temperature and solvent dependence. *Int. J. Chem. Kinet.* **1993**, *25*, 445–455. [[CrossRef](#)]
67. Westerhoff, P.; Mezyk, S.P.; Cooper, W.J.; Minakata, D. Electron pulse radiolysis determination of hydroxyl radical rate constants with Suwannee River fulvic acid and other dissolved organic matter isolates. *Environ. Sci. Technol.* **2007**, *41*, 4640–4646. [[CrossRef](#)]
68. Gara, P.M.D.; Bosio, G.N.; Gonzalez, M.C.; Russo, N.; del Carmen Michelini, M.; Diez, R.P.; Mártire, D.O. A combined theoretical and experimental study on the oxidation of fulvic acid by the sulfate radical anion. *Photochem. Photobiol. Sci.* **2009**, *8*, 992–997. [[CrossRef](#)] [[PubMed](#)]
69. Epling, G.A.; Lin, C. Investigation of retardation effects on the titanium dioxide photodegradation system. *Chemosphere* **2002**, *46*, 937–944. [[CrossRef](#)]
70. Van Doorslaer, X.; Dewulf, J.; De Maerschalk, J.; Van Langenhove, H.; Demeestere, K. Heterogeneous photocatalysis of moxifloxacin in hospital effluent: Effect of selected matrix constituents. *Chem. Eng. J.* **2015**, *261*, 9–16. [[CrossRef](#)]
71. Pelaez, M.; Falaras, P.; Likodimos, V.; Kontos, A.G.; Armah, A.; O’Shea, K.; Dionysiou, D.D. Synthesis, structural characterization and evaluation of sol–gel-based NF-TiO₂ films with visible light-photoactivation for the removal of microcystin-LR. *Appl. Catal. B Environ.* **2010**, *99*, 378–387. [[CrossRef](#)]
72. Hung, C.-H.; Yuan, C.; Li, H.-W. Photodegradation of diethyl phthalate with PANi/CNT/TiO₂ immobilized on glass plate irradiated with visible light and simulated sunlight-effect of synthesized method and pH. *J. Hazard. Mater.* **2017**, *322*, 243–253. [[CrossRef](#)] [[PubMed](#)]
73. Liang, C.; Huang, C.-F.; Mohanty, N.; Kurakalva, R.M. A rapid spectrophotometric determination of persulfate anion in ISCO. *Chemosphere* **2008**, *73*, 1540–1543. [[CrossRef](#)] [[PubMed](#)]
74. Allen, A.O.; Hochanadel, C.; Ghormley, J.; Davis, T. Decomposition of water and aqueous solutions under mixed fast neutron and γ -radiation. *J. Phys. Chem.* **1952**, *56*, 575–586. [[CrossRef](#)]
75. Huang, Y.; Han, C.; Liu, Y.; Nadagouda, M.N.; Machala, L.; O’Shea, K.E.; Sharma, V.K.; Dionysiou, D.D. Degradation of atrazine by Zn_xCu_{1-x}Fe₂O₄ nanomaterial-catalyzed sulfite under UV–vis light irradiation: Green strategy to generate SO₄^{•−}. *Appl. Catal. B Environ.* **2018**, *221*, 380–392. [[CrossRef](#)]
76. Lepentsiotis, V.; van Eldik, R.; Prinsloo, F.F.; Pienaar, J.J. A kinetic study of the redox behaviour of Fe-III(TPPS) TPPS=5,10,15,20-tetrakis(p-sulfonato)porphyrinate in the presence of peroxy monosulfate, hydrogen peroxide, and sulfite/oxygen. Direct evidence for multiple redox cycling and suggested mechanisms. *J. Chem. Soc.-Dalton Trans.* **1999**, 2759–2767. [[CrossRef](#)]

